Spring 4-8-2013

Neural Crosstalk Between Sympathetic Nervous System and Sensory Circuits to Brown Adipose Tissue

Yang Liu

NEURAL CROSSTALK BETWEEN SYMPATHETIC NERVOUS SYSTEM AND SENSORY CIRCUITS TO BROWN ADIPOSE TISSUE

by

YANG LIU

Under the Direction of Dr. Timothy Bartness

ABSTRACT

Brown adipose tissue (BAT) is a critical organ for non-shivering thermogenesis, which is under control of both sympathetic and sensory neural innervation. We utilized both a retrograde sympathetic nerve tract tracer pseudorabies virus and an anterograde sensory tract tracer the H129 strain of herpes simplex virus-1 to locate individual neurons across the neuroaxis that are part of the SNS outflow from brain to interscapular BAT and are part of the sensory input to the brain. We found specific neuronal phenotype of the double-infected neurons distributed from the hindbrain to the forebrain with highest densities in several discrete brain regions: the paraventricular hypothalamus (PVH), lateral hypothalamus (LHA), parabrachial nucleus (PB) and raphe pallidus (RPa). The neuroanatomical reality of the SNS-sensory feedback loops suggests coordinated control of BAT thermogenesis at several sites and indicates plasticity of SNS-sensory crosstalk.

INDEX WORDS: Sympathetic nervous system, Sensory circuits, Brown adipose tissue, Viral tract tracing

NEURAL CROSSTALK BETWEEN SYMPATHETIC NERVOUS SYSTEM AND SENSORY CIRCUITS TO BROWN ADIPOSE TISSUE

by

YANG LIU

A Thesis Submitted in Partial Fulfillment of the Requirements for the Degree of

Master of Science

in the College of Arts and Sciences

Georgia State University

2013

NEURAL CROSSTALK BETWEEN SYMPATHETIC NERVOUS SYSTEM AND SENSORY CIRCUITS

TO BROWN ADIPOSE TISSUE

by

YANG LIU

Committee Chair: Dr. Timothy Bartness

Committee: Dr. Aaron Roseberry

Dr. Bingzhong Xue

Electronic Version Approved:

Office of Graduate Studies

College of Arts and Sciences

Georgia State University

May 2013

ACKNOWLEDGEMENTS

First I must thank Dr. Timothy Bartness for his patient and thorough advice throughout my graduate studies. I would particularly like to thank the members of my committee, Dr. Xue andDr. Roseberry, for their guidance and insights.Many thanks to Dr. Vitaly Ryu, you gave me all the support I needed at the right times. I wish all of you great success.

TABLE OF CONTENTS

ACKNOWLEDGEMENTS iv

LIST OF TABLES vi

LIST OF FIGURES vii

1 INTRODUCTION 1

2 MATERIALS and METHODS 2

3 RESULTS 5

4 DISCUSSION 19

REFERENCES 23

LIST OF TABLES

Table 1 Distribution of Sympathetic and Sensory Neurons across the Neuroaxis 15

LIST OF FIGURES

Figure 1.Photomicrographs Showing the Distribution of PRV152 and H129 in the PVN……7

Figure 2.Photomicrographs of DMH with PRV152-ir and H129-ir neurons 8

Figure 3.Pictures of LHA showing PRV152 and H129 infected neurons 9

Figure 4.Low and high magnification of PAG with PRV-ir and H129-ir neurons 10

Figure 5.PRV-ir and H129-ir neurons labeled at PB 11

Figure 6. PRV152 and H129 injection into IBAT led to double-labeled cells in RM and RPa 12

Figure 7.PRV-ir and H129-ir neurons labeled at NTS 13

Figure 8.Quantification of single- and double-infected cells in MPO, PVH, PAG, PB and RPa 14

Figure 9.Percentage of double-labeled cells at different brain areas 14

1 INTRODUCTION

Brown adipose tissue (BAT) is a critical organ for non-shivering thermogenesis in rodents and its physiological function is under direct control of the sympathetic nervous system (SNS) [1, 2]. BAT has minor, at best parasympathetic nervous system (PSNS) innervation and then in only two minor BAT depots (i.e., pericardial [3] and mediastinal BAT [4], but not the major depot – interscapular BAT[4].

Viral transneuronal tracing has long been used to define central neural circuits (for review see [5, 6]). We previously demonstrated that injections of PRV Bartha's K strain into interscapular BAT (IBAT)[7] defined the origins of the extensive sympathetic outflow to this tissue involving nodes in this circuitry across the neuroaxis. Moreover, we and others [8, 9]also found several phenotypes of central neurons representing and linking this efferent SNS outflow to BAT including neurons possessing melanocortin-4-receptors (MC4-R) and the long form of the leptin receptor (Ob-Rb), both of which are heavily implicated in the control of thermogenesis and energy balance more generally. Physiologically, cold-exposure increases the sympathetic drive to BAT, resulting in release of norepinephrine (NE) from the SNS postganglionic nerve terminals innervating BAT stimulating beta-3 adrenoceptors on brown adipocytes [10], activating an intracellular signaling cascade ultimately activating uncoupling protein-1 (UCP-1), the mitochondria protein that uncouples oxidative phosphorylation from electron transport [for review see: [11].

Although in other organs PSNS afferents play a critical role in providing the brain with tissue-specific sensory feedback information[12, 13], the sparse and often lack of PSNS innervation of BAT[4] virtually eliminates these afferents from consideration as a potential sensory feedback conduit from BAT to the brain, BAT does, however, appear to have sensory innervation. Specifically, IBAT has positive immunoreactivity (-ir) for two proven sensory neuropeptides, substance P and calcitonin gene-related peptide [14, 15]. Furthermore, in Siberian hamsters, injections of an anterograde transneuronal viral tract tracer, the H129 strain of herpes simplex virus 1 (HSV-1), into the IBAT identified the central sensory circuits from this tissue with labeled cells across the neuroaxis from hindbrain to forebrain[16]. Many

of the sites receiving sensory input from IBAT [16] we also identified as part of the SNS outflow from the CNS to the tissue as revealed by our PRV studies [7, 8]. Thus, this overlap in SNS and sensory circuit labeling across these two studies suggests the possibility of individual neurons that are part of the SNS outflow from brain to BAT that also receive sensory input from the tissue – that is, potential SNS-sensory feedback loops serving an anatomical basis for neural crosstalk between these neural systems innervating BAT. Although the exact role of the sensory nerves innervating BAT is unknown, the impairment of the thermogenic response of BAT to acute cold exposure due to sensory denervation accomplished via local IBAT injection of capsaicin, the specific sensory neurotoxin[17, 18], strongly suggests sensory innervation of the tissue is necessary for the optimal physiological function of the BAT [16]. Therefore, we hypothesized that BAT SNS-sensory feedback loops might exist and tested this neuroanatomically by injecting both the sensory-specific transneuronal tract tracer, H129, and the SNS-specific transneuronal tract tracer, PRV, into IBAT to identify these neurons.

2 MATERIALS and METHODS

Animals.Male Siberian hamsters (*Phodopus sungorus*; ~3-4 mo old) from our breeding colony were single-housed in a long day photoperiod (16h: 8h light: dark cycle; at 21 ± 2 ºC) with free access to water and regular chow for 1 week before viral injections. All procedures were approved by the Georgia State University Institutional Animal Care and Use Committee and are in accordance with Public Health Service and United States Department of Agriculture guidelines.

Viral injections. Hamsters (n=8) were anesthetized with isoflurane and the left BAT pad was exposed for a series of PRV152 nanoinjections (7.5X 10^7 pfu/ml) into five loci (150 nl/loci) evenly distributed across the BAT depot. After 24 hours, the same BAT pad received injection of 750 nl of H129 (7.5X 10^7 pfu/ml) in the same manner described above. The syringe was held in place for 60 s to prevent efflux of virus after each injection. Finally, the incision was closed with sterile sutures and would clips, and

nitrofurozone powder (nfz Puffer; Hess & Clark, Lexington, KY) was applied locally to minimize the risk of bacterial infection. It is worth noting, that previously we demonstrated that surgical isolation of the fat pad from the surrounding tissues before H129 injections resulted in a pattern of infection indistinguishable from that of pads injected in their natural *in situ* position and condition suggesting the infections came directly from sensory nerves innervating the fat pad, but not surrounding tissues [C.K. Song and T.J. Bartness, unpublished observation]. In addition, the virus infections of the spinal cords were used as positive controls as PRV52 and H129 can individually infect spinal cord neurons {Bamshad, 1999 5573 /id; Vaughan, 2012 17324 /id}. Briefly, following injections of both viruses, the spinal cords were isolated, post-fixed in 4% paraformaldehyde for 2-3 hours, transferred to a 30% sucrose solution with 0.1% sodium azide and stored at 4°C. All spinal cords were longitudinally sectioned on a cryostat (Leica Microsystems Inc., Bannockburn, IL) into 20-µm serial sections and mounted on three glass slides (Superfrost Plus; VWR International, West Chester, PA) with every fourth section on the same slide. Generally, this procedure yielded 18-21 sections per the spinal cord, with each slide containing six to seven 20-µm sections. Sections were dried and stored at 4 °C until IHC.

Tissue fixation and sectioning. Animals were terminated 5 days after the last H129 injections, 6 days after the last PRV injections based on progression of both viruses to the brain. Hamsters were overdosed with pentobarbital sodium (Sleep Away; 300 mg/kg) and perfused transcardially with 0.02% heparinized saline first and then with 4% paraformaldehyde in 0.1 M phosphate buffer (PB; pH 7.4). The brains were collected and post-fixed in the same fixative overnight at 4°C, then transferred to a 30% sucrose solution with 0.1% sodium azide and stored at 4°C until they were sectioned on a freezing stage sliding microtome at 30 µm. Sections were stored in 0.1 M phosphate buffered saline (PBS) solution with 0.1% sodium azide until processed for double immunofluorescence.

IHC. Sections were rinsed in PBS (3 x 5 min) followed by a 30 min blocking in 10% normal goat serum (NGS; Vector Laboratories, Burlingame, CA). Next, sections were incubated with a mixture of primary rabbit anti-HSV-1 antibody (1:1000; DakoCytomation, Carpinteria, CA) and mouse monoclonal anti-GFP antibody (1:500; Abcam, Cambridge, MA) overnight. Consequently, sections were incubated in biotinylated secondary goat anti-rabbit antibody (1:750; Vector Laboratories) for 2 h, and then in the mixture of Alexa-488 conjugated goat anti-mouse secondary antibody (1:400; Invitrogen, Carlsbad, CA) and the fluorophore Alexa-594 (1:500; Invitrogen) for 1 h at room temperature. For immunohistochemical controls, the primary antibody was omitted. Sections were mounted onto slides (Superfrost Plus) in ProLong Gold Antifade Reagent (Molecular Probes, Eugene, OR). Sections of spinal cords were rehydrated and processed for detection of H129 (anti-HSV-1 antibody, 1:100 dilution; Dako Cytomation,) and PRV152 (anti-GFP antibody, 1:200 dilution;) as described above.

Quantification analysis. Images were viewed and captured with a microscope equipped with a digital camera and appropriate filters for Alexa-594 and Alexa-488. Exhaustive counts of the SNS and sensory labeling in every sixth section throughout the entire brain were performed using 10x and 20x objectives and CellSens software (Olympus, info here please) tagging method. A mouse brain atlas[19] was used to identify brain areas because no Siberian hamster brain atlas is commercially available and because of the similarity in size and shape of most of the brain structures between Siberian hamsters and mice. For the preparation of the photomicrographs, we used Adobe Photoshop CS3 to adjust only the brightness, contrast and sharpness and to make the composite plates.

Statistical Analyses. The percentage of double-labeled (-infected) neurons in the hypothalamus, mid-brain and hindbrain was analyzed by one-way repeated-measures ANOVA followed by the post hoc

Bonferroni's least significant difference (PLSD) using Sigma Stat 3.5 software (Systat Software, Chicago, IL). Significance was set at $P < 0.05$. All values are presented as means ± SEM.

3 RESULTS

Five out of eight animals were equally infected by both PRV152 and H129 neuronal tract tracers throughout the neuroaxis from the hindbrain to the forebrain and therefore are included in the study. No labeling was found when tissue was processed without the addition of primary antibody. We noticed both PRV152- and H129-labeled (-infected) neurons in the longitudinal sections of spinal cord (intermedial lateral horn and dorsal horn, respectively), as expected (data not shown).

The overall percentage of PRV152- and H129-ir double-labeled neurons in the forebrain were ~8.0%.The areas with extensive double-infected cells included the paraventricular nucleus of hypothalamus (PVH) (11.2±1.8 %; Fig. 1 and Table 1), dorsomedial hypothalamus (DMH) (9.8±2.4 %; Fig. 2 and Table 1), lateral hypothalamus (LHA) (9.3±0.6 %; Fig. 3 and Table 1), anterior hypothalamic nucleus (AHN) (8.9±1.0 %), posterior hypothalamic nucleus (PH) (11.1±1.5 %) and sub zona incerta (SubZI) (13.5±3.9 %; Table 1). The infected neurons were more heavily represented in the dorsal and ventral medial parvocellular subnuclei within the PVH (absolute numbers were 137.8±22.1 for PRV152-ir neurons and 129.8±32.8 for H129-ir neurons; Fig. 1). PRV152 infection in the SCH and the VMH was dominant over H129 infection.

The overall percentage of double-labeled neurons in the midbrain was ~9.8%. Double-labeled PRV152 + H129-ir neurons were found across the various midbrain regions, including the periaqueductal gray (PAG; 9.6±1.5 %; Fig. 4), ventral tegmental area (VTA; 7.6±2.8 %) and midbrain trigeminal nucleus (MEV; 12.9±5.0%).

Overall, the percentage of double-labeled neurons in the hindbrain was ~10.1%. Both single- and double-labeled neurons were notably present in the hindbrain. Some of the hindbrain areas with the highest numbers of PRV152- and H129-ir cells include the parabrachial nucleus (PB; 12.1±1.8 %; Fig. 5), locus ceruleus (LC; 8.5±2.4 %), the principal sensory nucleus of the trigeminal (PSV; 11.3±0.8 %), and motor

nucleus of trigeminal (V; 10.2±1.0 %), the raphe pallidus (RPa; 12.6±1.1 %; Fig. 6), raphe obscurus (RO; 12.9±1.4 %), the inferior olivary complex (IO; 9.8±1.8 %), raphe magnus (RM; 11.4±1.2 %), lateral reticular nucleus (LRN; 9.4±1.0 %), paragigantocellular reticular nucleus (PGRN; 10.3±1.9 %) , magnocellular reticular nucleus (MARN; 9.2±1.0 %), the facial motor nucleus (VII; 10.4±1.3 %) and the nucleus of the solitary tract (NTS; 7.3±1.4 %; Fig. 7).

In the forebrain, the medial preoptic area (MPO) had significantly higher absolute numbers of PRV152-ir neurons as compared with those infected with H129 (PRV 79.8±8.9 vs. H129 6.4±3.0, $p<0.01$; Fig. 8). The H129 immunostaining was suggestively decreased compared to PRV152 immunostaining in other forebrain areas such as medial preoptic nucleus (MPN), lateral preoptic area (LPO) and anteroventral preoptic nucleus (AVP); however without statistical significance (Table-1). The percentage of double-labeled neurons in the preoptic areas (~3.5 %) was significantly lower than those in the forebrain, midbrain and hindbrain ($p<0.05$). There was no statistical difference between the numbers of PRV152/H129 colocalized neurons in the three major brain regions examined (Fig. 9)

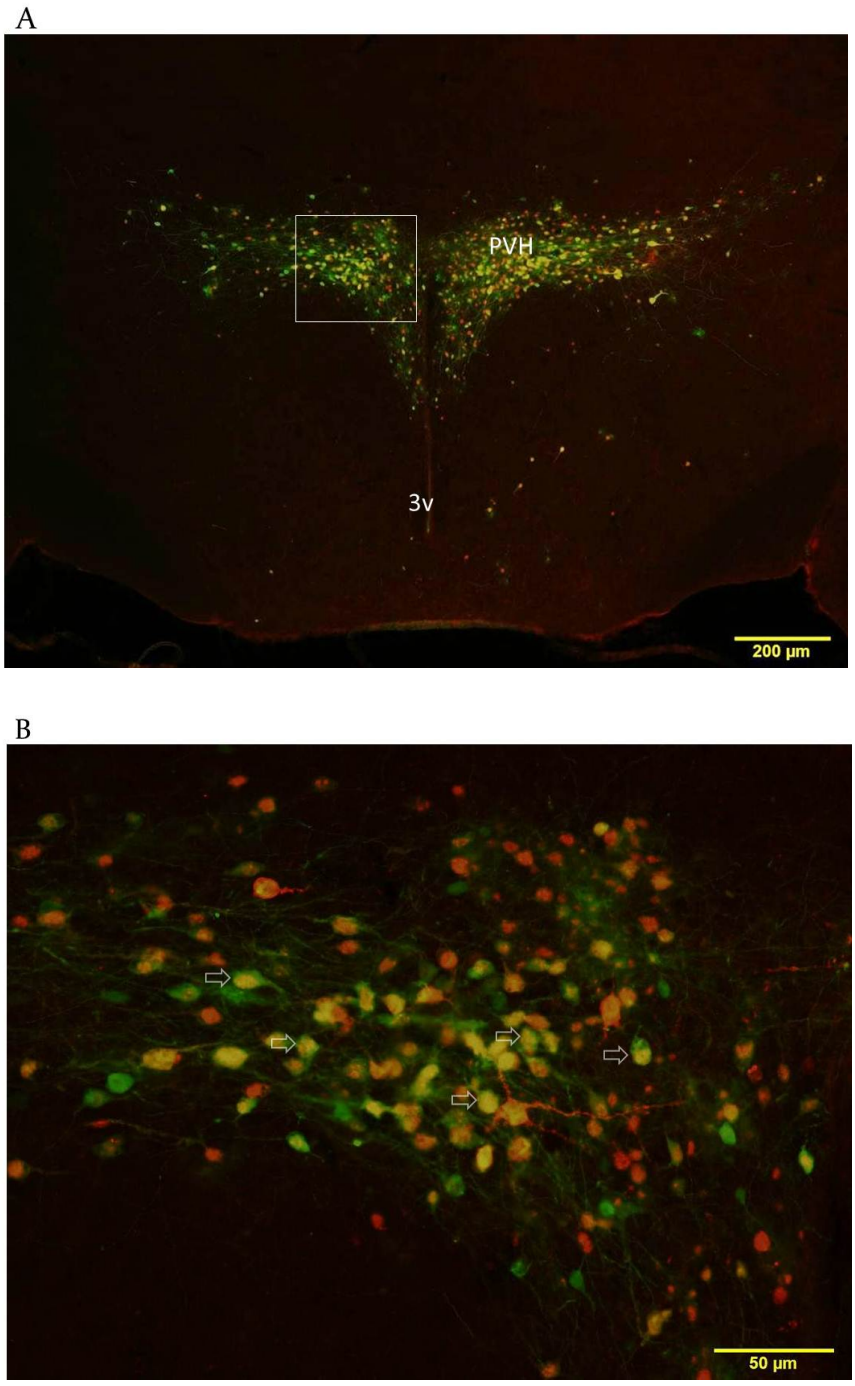

Figure 1. Photomicrographs showing the distribution of PRV152 and H129 in the PVN of the Siberian hamster. *A*: Low magnification (4x) photomicrograph of the PVN *B*: High magnification (20x) of the area outlined in *A*. Open arrows indicate double-labeled cells. Scale bar = 200 µm in *A*; 50 µm in *B*. 3v: third ventricle

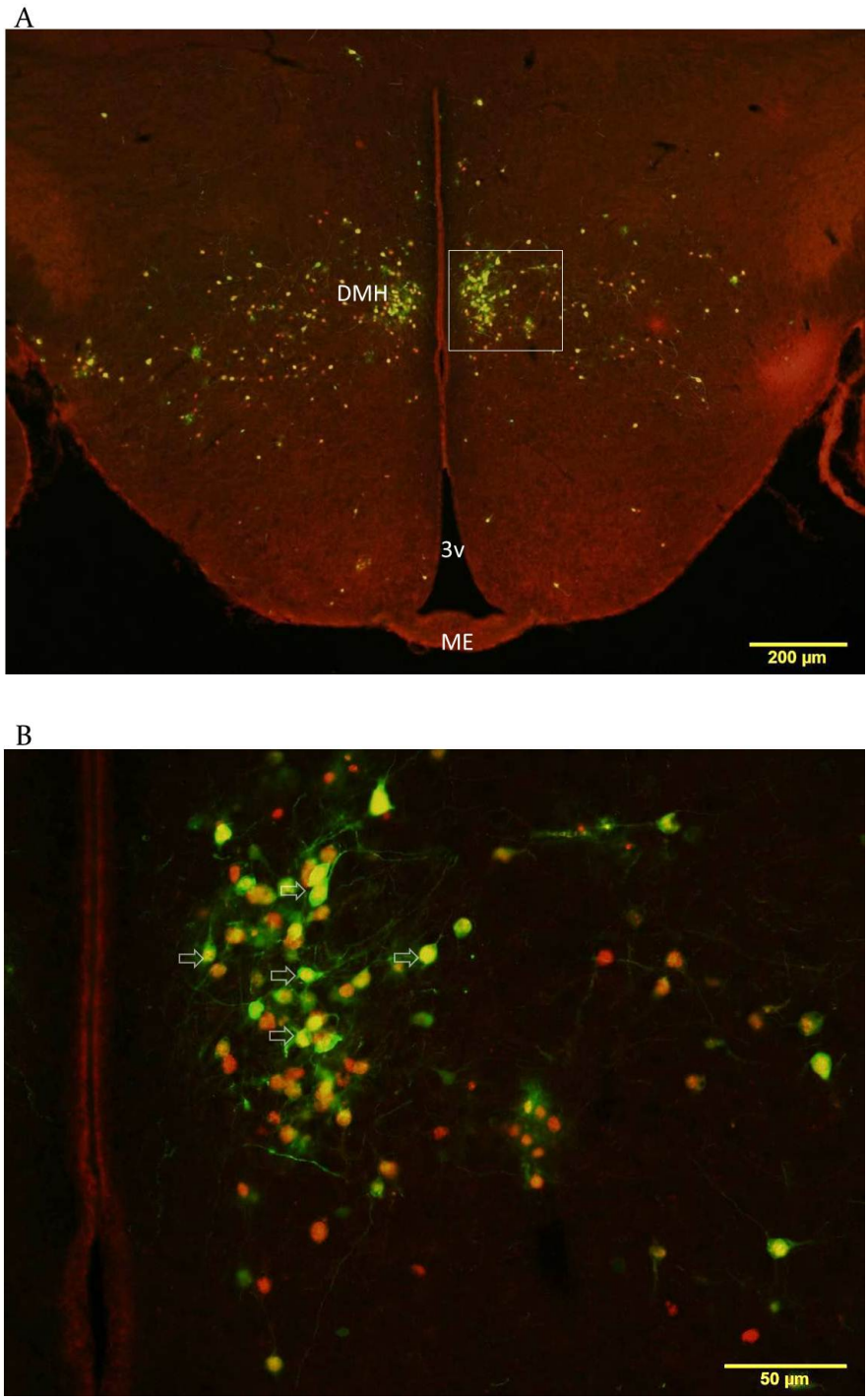

Figure 2. Photomicrographs of dorsomedial hypothalamic nucleus (DMH) with PRV152-ir and H129-ir neurons. *A*: Low magnification (4x) graph of DMH: *B*: Higher magnification (20x) graph of area outlined in *A*. Double-labeled cells are indicated by the open arrows. Scale bar = 200 µm in *A*; 50 µm in *B*. 3v: third ventricle; ME: median eminence

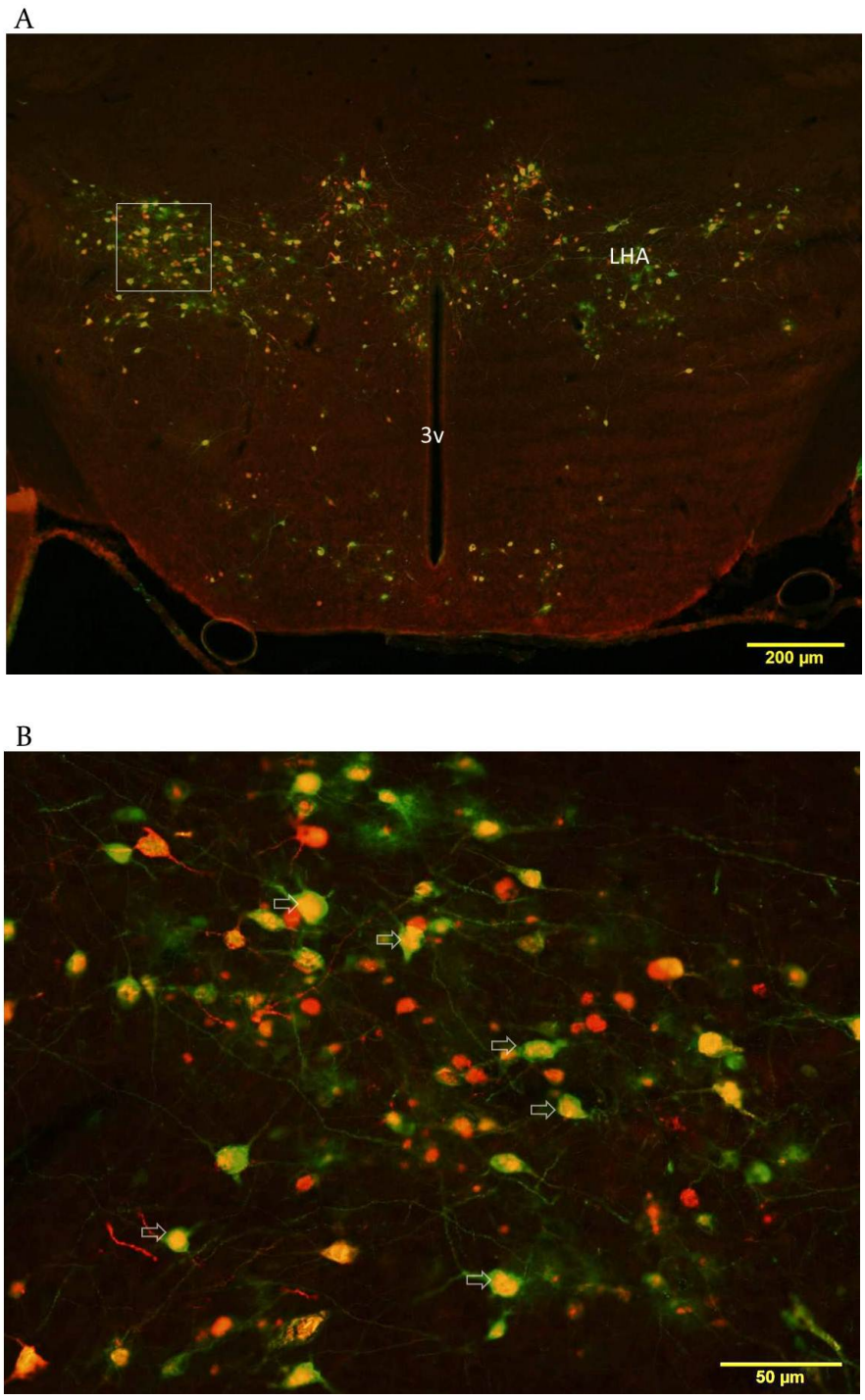

Figure 3. Pictures of LHA showing PRV152 and H129 infected neurons. *A*: Low magnification photomicrograph (4x) of LHA. *B*: Higher magnification (20x) picture of area outlined in *A*. Double-labeled cells are noted by the open arrows. Scale bar = 200 µm in *A*; 50 µm in *B*.

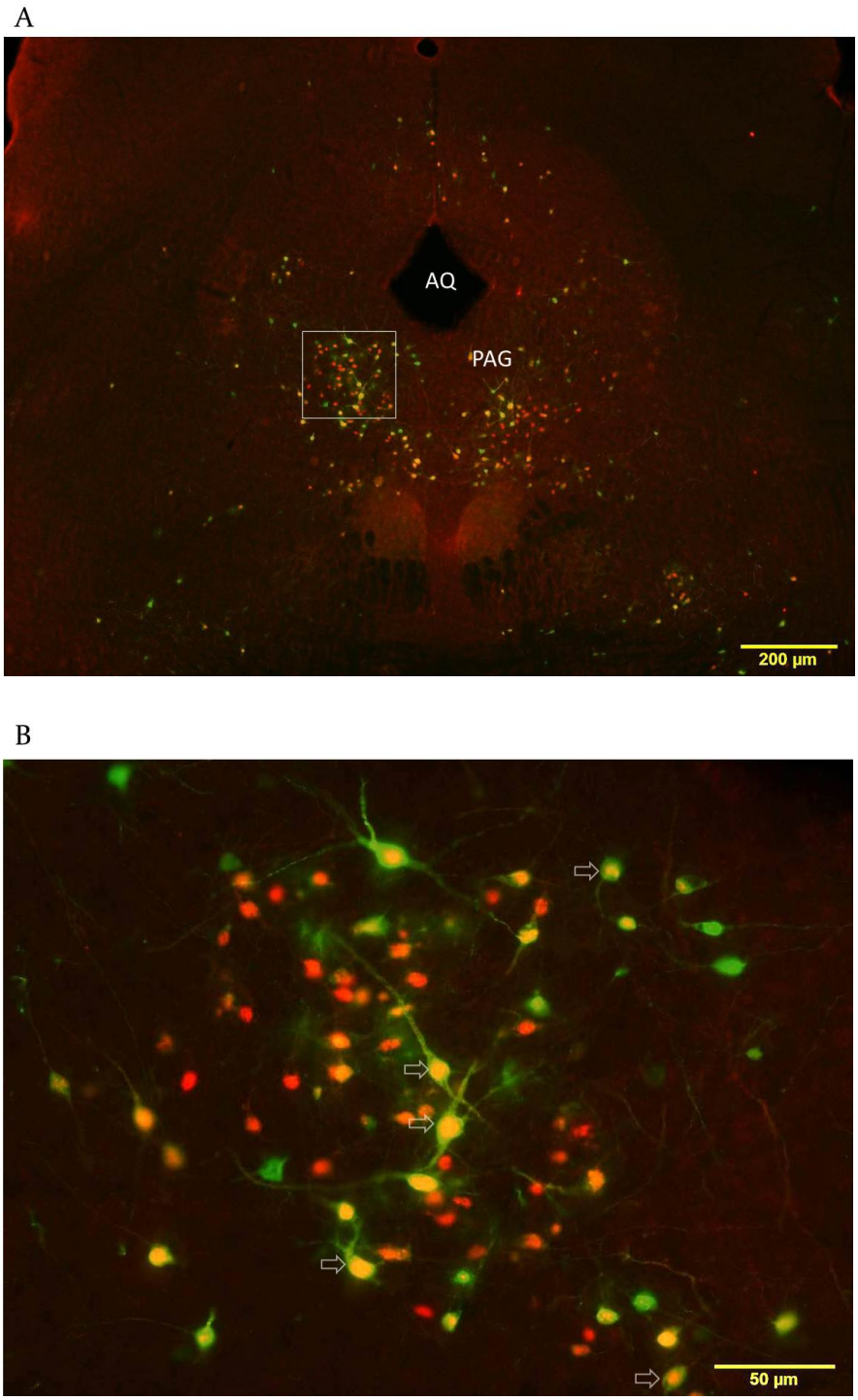

Figure 4. Low and high magnification of midbrain at the level of the periaqueductal gray (PAG) with PRV-ir and H129-ir neurons. *A*: 4x magnification of graph of PAG; *B*: 20x magnification graph of area outlined shown in *A*. Open arrows= double-labeled cells. Scale bar = 200 µm in *A*; 50 µm in *B*. AQ: cerebral aqueduct

A

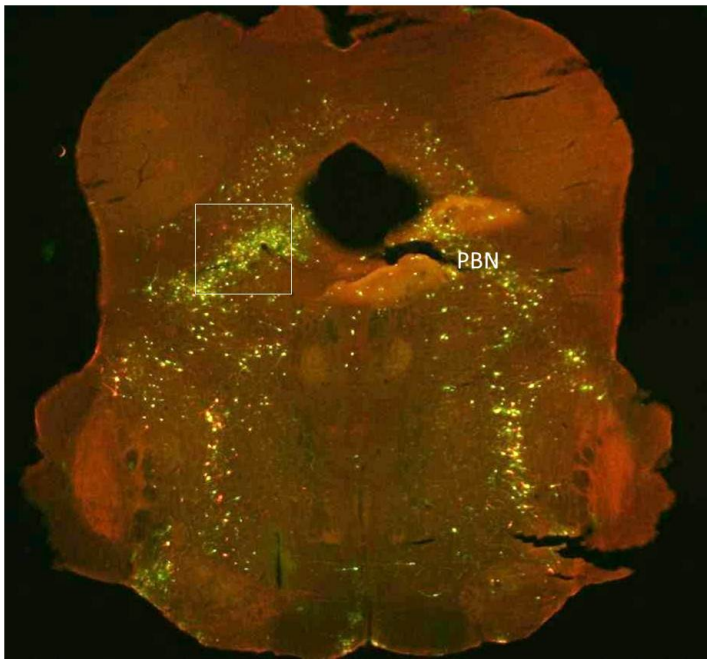

B

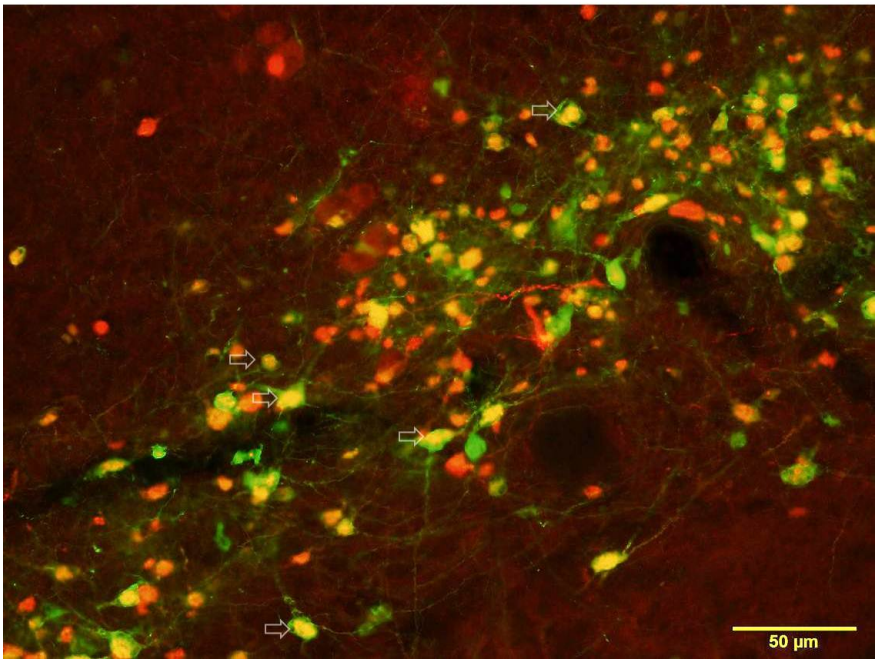

Figure 5. PRV-ir and H129-ir neurons labeled at parabrachial nucleus (PB). *A*: low magnification (4x) of PBN; *B*: higher magnification (20x) picture of area outlined shown in A. Open arrows= double-labeled cells. Scale bar = 200 µm in *A*; 50 µm in *B*.

A

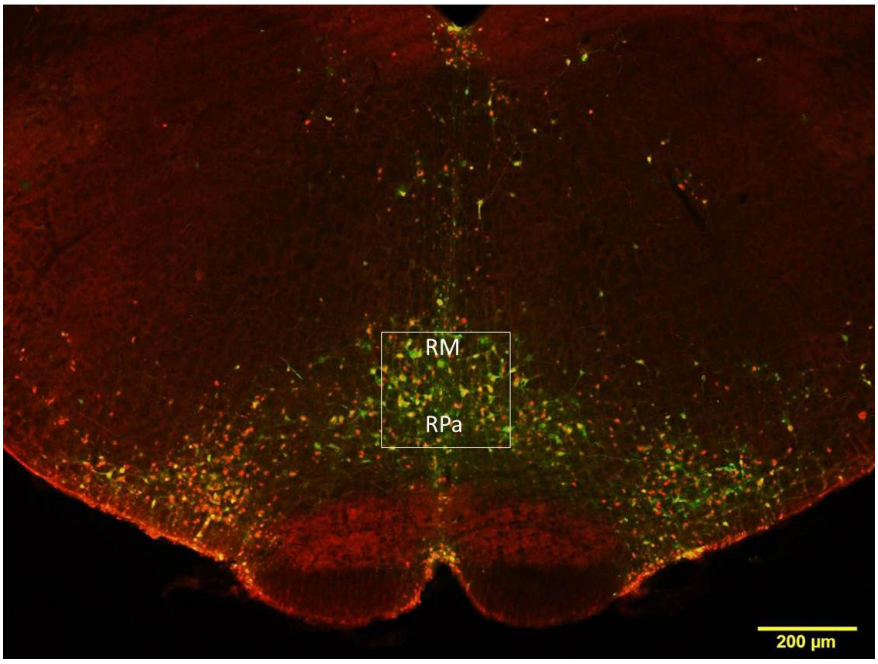

B

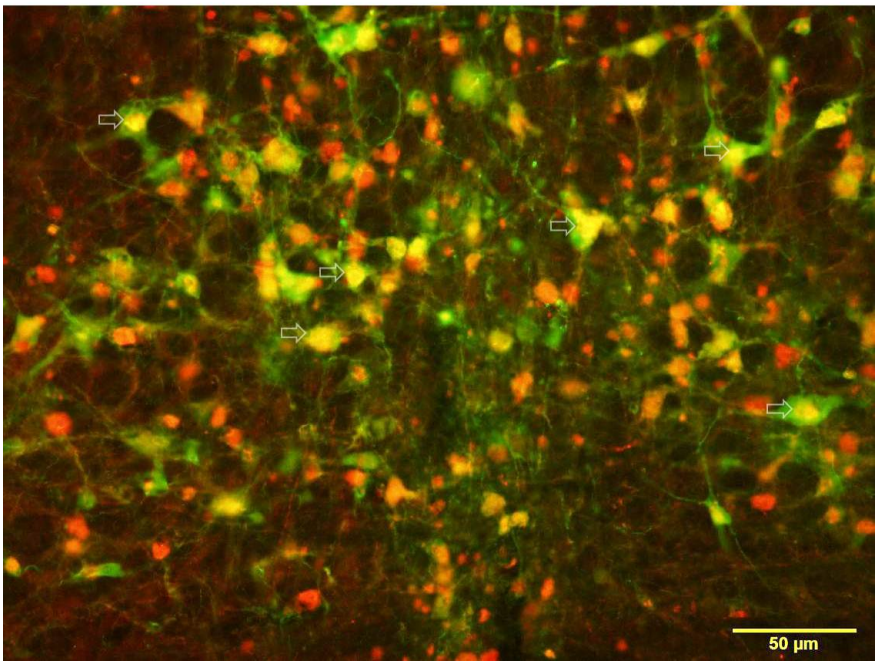

Figure 6. PRV152 and H129 injection into IBAT led to double-labeled cells in RM and RPa *A*: Low magnification (4x) picture; *B*: Regions outlined in A under higher magnification (20x). Open arrows= double-labeled cells. Scale bar = 200 µm in *A*; 50 µm in *B*.

A

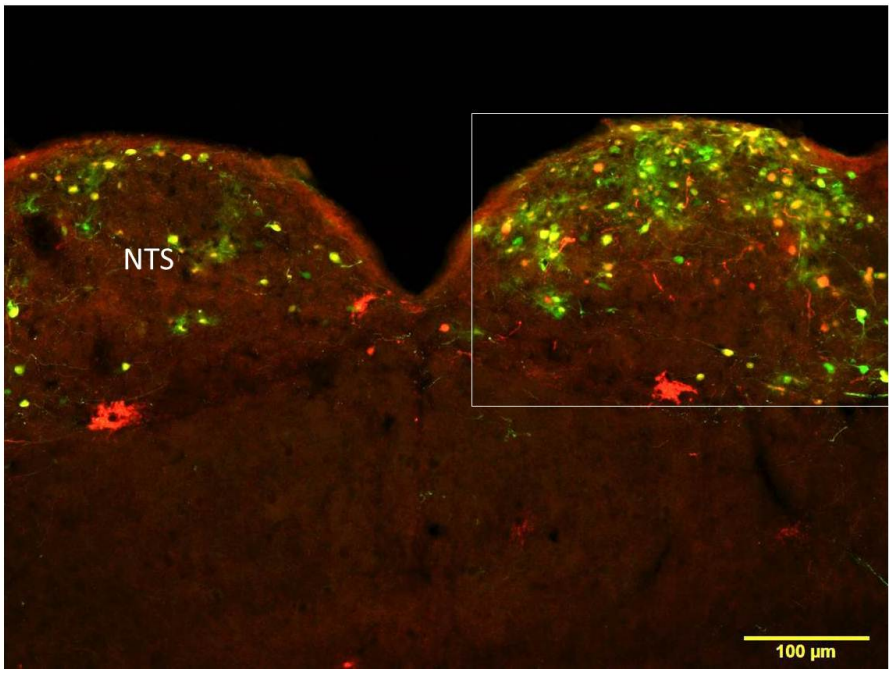

B

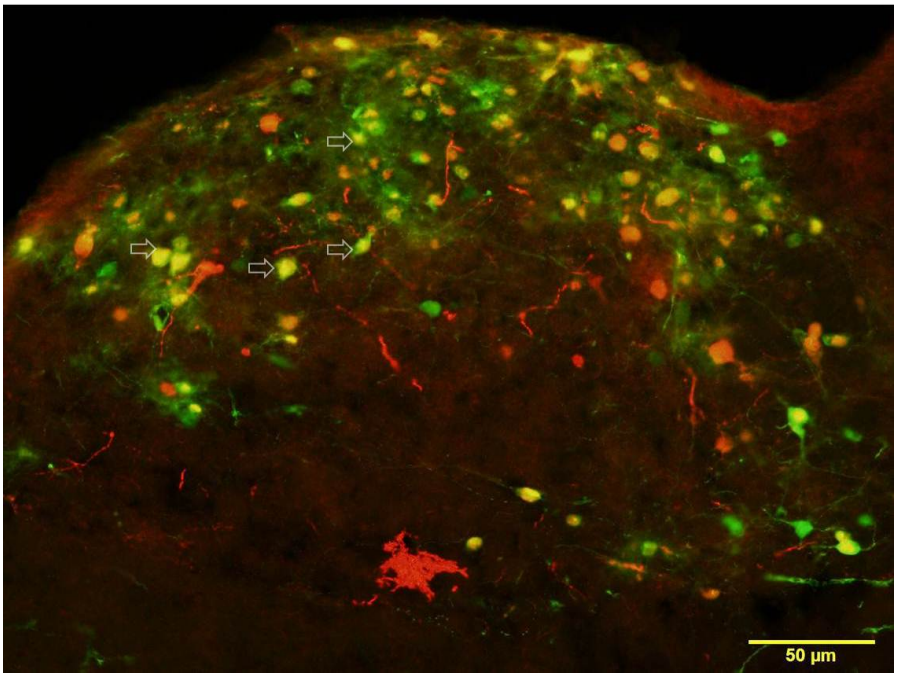

Figure 7. PRV-ir and H129-ir neurons labeled at nucleus of solitary tract (NTS). *A*: low magnification (10x) of NTS; *B*: higher magnification (20x) picture of area outlined shown in A. Open arrows= double-labeled cells. Scale bar = 100 µm in *A*; 50 µm in *B*.

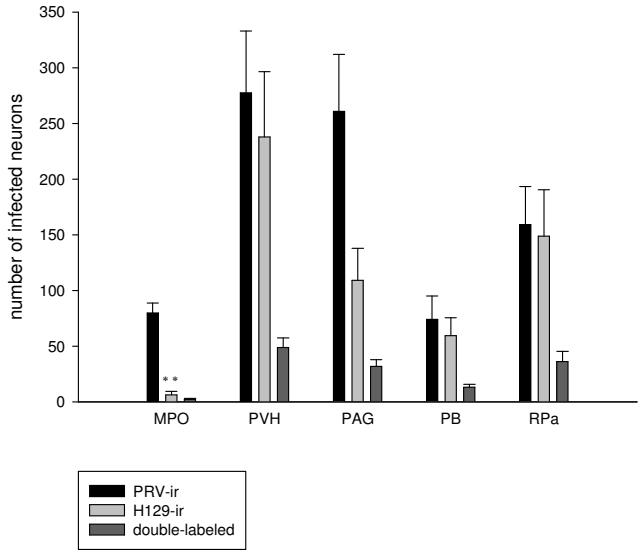

Figure 8. Quantification of H129- and PRV152-ir neurons in the MPO, PVH, PAG, PB and RPa. More PRV152-ir cells were found in MPO in comparison with H129-ir cells (* $p<0.01$). The number of H129-ir cells in PAG seemed to be less than PRV152-ir cells, however without statistical significance ($p=0.07$).

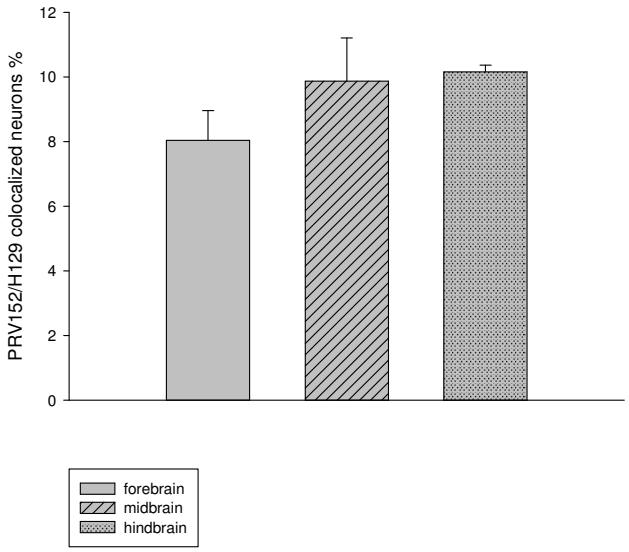

Figure 9. Percentage of double-labeled H129+PRV152-ir neurons in forebrain, midbrain and hindbrain. No significant difference was found regardless of any brain areas examined.

Table 1: Distribution of sympathetic and sensory neurons across the neuroaxis.

	No. of PRV-labeled cells	No. of H129-labeled cells	No. of Double-labeled cells	% of Double-labeled cells
Forebrain				
MPO	79.8±8.9	6.4±3.0**	2.2±1.0	3.0±1.7
MPN	36.4±13.8	6.8±2.6	1.4±0.9	5.0±3.0
MEPO	17.4±5.2	0.8±0.8	0.2±0.2	2.0±2.0
LPO	23.8±10.5	1.5±0.8	0.8±0.4	1.7±1.0
AVP	32.6±9.5	7.8±5.9	1.4±1.0	2.8±1.7
AVPV	23.5±7.9	3.3±1.8	1.3±0.8	3.3±2.3
SCH	13.5±6.9	4.5±1.7	0.5±0.4	1.2±1.0
AHNa	7.4±2.2	3.8±2.2	1±0.4	9.2±4.3
AHNp	22.8±9.1	9.8±5.5*	2.4±1.3	5.8±2.4
PVH	277.4±55.5	237.8±58.7	48.8±8.7	11.2±1.8
PVHpv	15.0±4.9	14.8±7.2	3.5±1.7	10.7±3.2
PVHdp	30.6±7.3	36.4±11.3	6.2±1.7	8.9±3.1
PVHmpd	137.8±22.1	129.8±32.8	23.6±4.2	10.4±1.7
PVHmm	12.2±4.9	7.2±2.3	1.8±1.1	6.8±4.5
PVHpml	36.0±6.8	35.3±10.7	5.8±1.7	8.5±1.4
PVHmpv	16.7±2.5	16.3±4.2	3.3±1.4	12.6±5.8
PVHlp	22.7±12.0	25.4±12.5	7.6±5.2	8.4±2.3
ARH	19.6±7.1	8.2±2.1	2.0±0.9	5.9±2.6
LHA	101.6±20.8	40.0±3.9	11.8±1.7	9.3±0.6
VMH	6.4±4.1	0	0	0
DMH	83.3±31.8	30.3±5.8	8.7±1.7	9.8±2.3
PH	39.8±12.9	15.8±1.5	5.0±1.1	11.1±1.5

ZI	18±11.0	8.6±4.5	1.2±0.8	2.6±1.7
SubZI	31.6±4.6	22.4±8.9	6.8±2.0	13.5±3.9
Midbrain				
PAG	260.6±51.4	109.2±28.8	32.0±5.8	9.6±1.5
dmPAG	32.4±9.3	12.2±4.7	2.8±1.1	6.3±1.2
dlPAG	26.0±6.1	8.4±2.6*	1.8±0.7	5.1±1.6
lPAG	60.0±11.5	30.0±6.9*	8.8±1.3	11.5±2.1
vlPAG	54.8±11.6	18.2±6.0	6.4±1.4	10.3±1.8
DR	23.6±6.7	7.0±2.2*	2.4±0.6	7.7±2.4
MRN	54.3±20.3	19.0±6.4	6.0±1.9	8.5±3.1
RN	18.0±5.5	9.6±2.9	2.6±0.2	12.5±3.3
VTA	32.5±12.7	13.5±4.6	3.5±1.2	7.6±2.8
MEV	15.7±4.5	7.3±2.5	2.7±1.4	12.9±5.0
Hindbrain				
PRNr	38.0±16.0	27.4±9.6	6.4±2.5	11.3±1.1
PRNc	51.4±15.1	42.6±8.1	9.2±2.5	10.6±1.9
PB	74.2±20.8	59.6±16.1	13.2±2.4	12.1±1.8
PBmm	36.6±10.3	40.5±8.4	7.6±1.5	12.7±1.1
PBls	6.3±2.9	5.3±1.6	1.7±0.8	7.3±4.7
PBlc	23.6±7.1	13.4±5.3	3.0±1.2	9.5±4.3
PBle	11.3±5.6	11.3±4.7	2.0±0.7	8.0±2.6
LC	29.8±9.9	28.3±5.7	5.0±1.5	8.5±2.4
B	16.3±6.6	9.7±4.6	3.8±1.2	20.6±5.9
PSV	29.0±13.3	26.8±9.6	5.5±2.3	11.3±0.8
LDT	13.3±4.6	4.3±0.7	1.7±0.7	12.3±7.0
V	18.7±3.3	20.7±1.1	3.7±0.5	10.2±1.0

RM	83.8±25.9	87.2±17.7	17.2±4.1	11.4±1.2
RPa	159.2±34.0	148.8±41.6	36.2±9.2	12.6±1.1
RO	154.5±55.9	116.0±14.1	30.5±5.0	12.9±1.4
GRN	52.8±28.8	39.0±13.5	6.2±3.0	6.4±2.2
PGRNl	31.0±6.6	29.0±6.8	7.0±1.3	13.0±1.2
PGRNd	42.0±17.3	42.3±16.5	7.3±2.8	8.5±1.0
MARN	108.0±19.7	127.2±32.4	19.0±3.0	9.2±1.0
PARN	14.0±4.1	10.7±3.9	1.3±0.5	4.6±2.0
VII	67.4±12.1	57.6±19.5	11.8±3.0	10.4±1.3
IO	152.7±41.6	129.3±15.0	25.7±6.1	9.8±1.8
XII	24.3±5.2	17.0±8.0	0.7±0.3	1.9±1.0
LRNm	120.7±36.1	96.0±24.0	18.7±2.9	9.4±1.0
MDRNv	59.3±39.9	43.0±18.0	9.0±5.9	6.8±3.4
NTS	384.7±209.7	281.0±120.7	48.3±22.2	7.3±1.4
NTSm	167.3±82.0	126.0±54.5	20.7±11.3	6.2±2.0
NTSl	111.7±52.4	77.7±30.0	18.0±6.7	10.2±1.3
NTSco	158.5±75.5	116.0±9.8	14.5±0.4	6.5±2.0
PRP	25.5±11.2	15.0±6.6	3.8±2.8	6.2±3.1
DMX	16.0±8.2	14.5±1.2	2.0±1.6	5.7±4.7

Means ± SEM (n=5)

** p<0.01 vs. No. of PRV152-ir cells; * p<0.05 vs. No. of PRV152-ir cells

MPO, medial preoptic area; MPN, medial preoptic nucleus; MEPO, median preoptic nucleus; LPO, lateral preoptic area; AVP, anteroventral preoptic nucleus; AVPV, anteroventral periventricular nucleus; SCH, suprachiasmatic nucleus; AHNa, anterior hypothalamic nucleus, anterior part; AHNp, anterior hypothalamic nucleus, posterior part; PVH, paraventricular hypothalamic nucleus; PVHpv, paraventricular hypothalamic nucleus, parvicellular division, periventricular part; PVHdp, paraventricular hypothalamic nucleus, descending division, dorsal parvicellular part; PVHmpd, paraventricular hypothalamic nucleus, parvicellular

division, medial parvicellular part, dorsal zone; PVHmm, paraventricular hypothalamic nucleus, magnocellular division, medial magnocellular part; PVHpml, paraventricular hypothalamic nucleus, magnocellular division, posterior magnocellular part, lateral zone; PVHmpv, paraventricular hypothalamic nucleus, descending division, medial parvicellular part, ventral zone; PVHlp, paraventricular hypothalamic nucleus, descending division, lateral parvicellular part; ARH, arcuate nucleus; LHA, lateral hypothalamus; VMH, ventromedial hypothalamic nucleus; DMHa, dorsomedial nucleus of the hypothalamus, anterior part; DMHp, dorsomedial nucleus of the hypothalamus, posterior part; PH, posterior hypothalamic nucleus; ZI, zona incerta; SubZI, sub zona incerta; PAG, periaqueductal gray; dmPAG, dorsomedial periaqueductal gray; dlPAG, dorsolateral periaqueductal gray; lPAG; lateral periaqueductal gray; vlPAG, ventrolateral periaqueductal gray ; DR, dorsal raphe nucleus; MRN, midbrain reticular nucleus; RN; red nucleus; VTA, ventral tegmental area; PRNr, pontine reticular nucleus, rostral part; PRNc, pontine reticular nucleus, caudal part; NLL, nucleus of the lateral lemniscus; PBmm, parabrachial nucleus, medial division, medial part; PBls, parabrachial nucleus, lateral division, superior lateral part; PBlc, parabrachial nucleus, lateral division, central lateral part; PBle, parabrachial nucleus, lateral division, external lateral part; LC, locus ceruleus; B, Barrington's nucleus; MEV, midbrain trigeminal nucleus; PSV, principal sensory nucleus of the trigeminal; LDT, laterodorsal tegmental nucleus; V, motor nucleus of trigeminal; RM, nucleus raphe magnus; RPa, nucleus raphe pallidus; RO, nucleus raphe obscurus; GRN, gigantocellular reticular nucleus; PGRNl, paragigantocellular reticular nucleus, lateral part; PGRNd, paragigantocellular reticular nucleus, dorsal part; MARN, magnocellular reticular nucleus; PARN; parvicellular reticular nucleus; VII, facial motor nucleus; IO, inferior olivary complex; XII, hypoglossal nucleus; LRNm, lateral reticular nucleus, magnocellular part; MDRNv; medullary reticular nucleus, ventral part; NTSm, nucleus of the solitary tract, medial part; NTSl, nucleus of the solitary tract, lateral part; NTSco, nucleus of the solitary tract, commissural part; PRP, nucleus prepositus; DMX, dorsal motor nucleus of the vagus nerve

4 DISCUSSION

In the current study, we successfully applied two viral neural tract tracers, the sympathetic nerve-specific PRV152 and the sensory nerve-specific H129, into the IBAT of Siberian hamsters. We report here for the first time the presence of neural crosstalk between SNS and sensory neural innervation of the BAT, as evidenced by the co-localization of both neural tract tracers predominately in the PVH, DMH, LHA, PB, RPa and NTS brain regions. It should be noted that the number of double-labeled neurons likely has been underestimated here because an earlier infection with one virus could greatly reduce the susceptibility to infection by another virus if not completely preventing the second infection (the phenomenon of exclusion)[20]. Due to the unpredictable time interval for each virus to reach any specific area, the neurons on both ascending and descending pathways to the BAT may not necessarily show overlapped infections, despite the selection of inoculation and post inoculation time points that optimize the double-viral technique by matching viral rates of progression through the neural axis as closely as possible [7, 8, 16]. Nevertheless, the data in this study provide the meaningful insight into the distributed neural system integrating SNS and sensory neural circuits innervating IBAT based the demonstration of doubly infected neurons (i.e., possible SNS-sensory neural feedback loop neurons).

The MPO of the forebrain is involved in the SNS outflow to the IBAT and shown to control the thermoregulatory responses to skin-cooling in several organs including the BAT[21]. In the present study, we found that the MPO area was predominantly represented as part of the SNS outflow to, but not the sensory inflow from IBAT. This apparent dominant innervation of the sympathetic outflow over the sensory inflow to the MPOA is in accordance with our previous finding of relatively sparse MPOA H129-infected neurons relative to many other areas [16]and impressive PRV152-infected neurons [7, 8, 22]. Despite the relatively lesser contribution of sensory circuit neurons in the MPO, this by no means lessens the contribution of the sensory circuit responding to the thermoregulatory signaling from the skin as the MPOA-sensory innervation in the present study mainly reflects the sensory pathway originating from

the IBAT. Because IBAT increases thermogenesis in response to cold-exposure in decerebrated rats, where most of the midbrain and all of the forebrain including, of course, the MPOA, are disconnected from the hindbrain [23], the necessity of sensory input to the MPO or other rostral brain sites combined with the presence of PRV152+H129 dually infected neurons in the hindbrain, seems to indicate that, unlike some of the models proposed for thermoregulation and the sympathetic control of BAT where the MPOA is depicted as the 'origin' of the descending signals and recipient of the ascending afferent information [24], sensory input may crosstalk with central sympathetic outflow across the neuroaxis including the hindbrain.

In the present study, hypothalamic areas with the highest percentages of double-labeled PRV152 and H129 neurons included the PVH, DMH and LHA. Previously, we demonstrated that SNS outflow to the IBAT comprises a group of PVH MC4-R neurons and that intra-PVH infusion of MC3/4-R agonist increases IBAT temperature[8]. The phenotypic characterization of the IBAT sensory MC4-R possessing neurons within the PVH as well as the DMH and the LHA that also are part of the SNS outflow to BAT is a topic for future investigations.

In the midbrain and the hindbrain, PRV152- and H129-ir double-labeled cells were notably present in the PAG, PB, RPa, and the NTS, all of which can affect the SNS activity to IBAT individually [25-28]. The PAG receives afferent fibers not only from the PB and the RPa [29], but from the spinal cord as well[30]. The PVH, DMH and LHA all receive afferent projections from the PB and the NTS [31-34]. As with other critical biological functions, such as energy intake [35], these systems appear to be distributed across the neuroaxis and the pattern of double-labeled neurons in the present study is one of many demonstrations that this is true for thermogenesis in general and BAT thermogenesis specifically with afferents and efferents in the forebrain, midbrain and hindbrain.

Our previous study demonstrated that the intact sensory nerves on BAT are necessary for its thermogenic function, at least during acute cold-exposure [16]. To our knowledge, no molecular signal

from BAT responsible for the activation of local sensory nerve terminals has been identified at this time. In this regard, we previously reported[36]that the firing frequency of decentralized sensory nerve fibers innervating inguinal white adipose tissue (IWAT) was markedly increased when the anesthetized hamsters were injected with the glucoprivic agent 2-deoxy-D-glucose known to drive sympathetic outflow and lipolysis[37]suggesting that factors associated with activation of β-adrenoceptors might activate afferents, perhaps associated with lipolysis (e.g., fatty acids, glycerol). Indeed, in terms of BAT, lipolysis is necessary for the full effect of NE-induced BAT thermogenesis, as mice with the elimination of all protein kinase A phosphorylation sites on the adipocyte intracellular protein perilipin have an abolished NE-induced lipolytic response in isolated brown adipocytes and a severely blunted (~70%) decrease in NE-induced thermogenesis in vivo [38].

From the perspective of plausible BAT SNS-sensory feedback loops, such an entity could be involved in controlling the marked increases in blood flow to BAT with thermogenic challenges seen in Siberian hamsters, and laboratory rats and mice (~15-100 fold or more)[39-41]and a role for sensory feedback in the control of local blood flow has been repeatedly proposed [42, 43]. Therefore, there could be more than one population of sensory nerves innervating the BAT with some activated by the changes of local temperature (evidenced in other organs[44]), others responding to changes in blood flow and still other lipolysis-related factors.

In the present study, we found that the highest percentage of double-labeled neurons reaches ~10 % in several regions of the hypothalamus, midbrain or hindbrain. Compared with more than half of double-labeled neurons in many of the same and other brain areas following injections of PRV152 and H129 into the IWAT (Ryu and Bartness, unpublished data), the lower rate of double-labeled neurons seems to be in contradiction with the higher density of SNS innervation of the BAT, but may reflect a lesser number of functions for this tissue versus WAT. The phenotypic identification of the double- and single-

labeled neurons as well as the nature of the sensory stimulus activating the sensory neurons is currently under investigation.

Collectively, the overlapping of the SNS and sensory neurons innervating IBAT indicates crosstalk between the SNS efferent and sensory afferent neural controls of this tissue and these individual neurons found to be dually infected at several regions across the neuroaxis in this study suggest the neuroanatomical reality of the BAT SNS-sensory neural feedback loops and/or a coordinated or multiple redundant control of thermoregulatory functions.

REFERENCES

1. Bartness, T. J.; Vaughan, C. H.; Song, C. K. Sympathetic and sensory innervation of brown adipose tissue. Int. J Obes. (Lond) 2010, 34 Suppl 1:S36-S42.

2. van Marken, L. W. Human brown fat and obesity: methodological aspects. Front Endocrinol. (Lausanne) 2011, 2:52.

3. Schafer, M. K.; Eiden, L. E.; Weihe, E. Cholinergic neurons and terminal fields revealed by immunohistochemistry for the vesicular acetylcholine transporter. II. The peripheral nervous system. Neuroscience 1998, 84:361-376.

4. Giordano, A.; Frontini, A.; Castellucci, M.; Cinti, S. Presence and distribution of cholinergic nerves in rat mediastinal brown adipose tissue. J. Histochem. Cytochem. 2004, 52:923-930.

5. Song, C. K.; Enquist, L. W.; Bartness, T. J. New developments in tracing neural circuits with herpesviruses. Virus Res. 2005, 111:235-249.

6. Enquist, L. W. Exploiting circuit-specific spread of pseudorabies virus in the central nervous system: insights to pathogenesis and circuit tracers. J. Infect. Dis. 2002, 186 Suppl 2:S209-S214.

7. Bamshad, M.; Song, C. K.; Bartness, T. J. CNS origins of the sympathetic nervous system outflow to brown adipose tissue. Am. J. Physiol. 1999, 276:R1569-R1578.

8. Song, C. K.; Vaughan, C. H.; Keen-Rhinehart, E.; Harris, R. B.; Richard, D.; Bartness, T. J. Melanocortin-4 receptor mRNA expressed in sympathetic outflow neurons to brown adipose tissue: Neuroanatomical and functional evidence. Am. J. Physiol. 2008, 295:R417-R428.

9. Oldfield, B. J.; Giles, M. E.; Watson, A.; Anderson, C.; Colvill, L. M.; McKinley, M. J. The neurochemical characterisation of hypothalamic pathways projecting polysynaptically to brown adipose tissue in the rat. Neuroscience 2002, 110:515-526.

10. Zhao, J.; Unelius, L.; Bengtsson, T.; Cannon, B.; Nedergaard, J. Coexisting beta-adrenoceptor subtypes: significance for thermogenic process in brown fat cells. Am. J. Physiol 1994, 267:C969-C979.

11. Cannon, B.; Nedergaard, J. Brown adipose tissue: function and physiological significance. Physiol Rev. 2004, 84:277-359.

12. Berthoud, H. R. The vagus nerve, food intake and obesity. Regul. Pept. 2008, 149:15-25.

13. Kubin, L.; Alheid, G. F.; Zuperku, E. J.; McCrimmon, D. R. Central pathways of pulmonary and lower airway vagal afferents. J. Appl. Physiol 2006, 101:618-627.

14. De, M. R.; Ricquier, D.; Cinti, S. TH-, NPY-, SP-, and CGRP-immunoreactive nerves in interscapular brown adipose tissue of adult rats acclimated at different temperatures: an immunohistochemical study. J. Neurocytol. 1998, 27:877-886.

15. Norman, D.; Mukherjee, S.; Symons, D.; Jung, R. T.; Lever, J. D. Neuropeptides in interscapular and perirenal brown adipose tissue in the rat: a plurality of innervation. J. Neurocytol. 1988, 17:305-311.

16. Vaughan, C. H.; Bartness, T. J. Anterograde transneuronal viral tract tracing reveals central sensory circuits from brown fat and sensory denervation alters its thermogenic responses. Am. J. Physiol Regul. Integr. Comp Physiol 2012, 302:R1049-R1058.

17. Jansco, G.; Kiraly, E.; Jansco-Gabor, A. Direct evidence for an axonal site of action of capsaicin. Nauyn-Schmiedeberg's Arch. Pharmacol. 1980, 31:91-94.

18. Jansco, G.; Kiraly, E.; Joo, F.; Such, G.; Nagy, A. Selective degeneration by capsaicin of a subpopulation of primary sensory neurons in the adult rat. Neurosci. Lett. 1985, 59:209-214.

19. Paxinos, G.; Franklin, K. B. J. The Mouse Brain in Stereotaxic Coordinates. 2nd ed. New York: Academic Press; 2007.

20. Kim, J. S.; Enquist, L. W.; Card, J. P. Circuit-specific coinfection of neurons in the rat central nervous system with two pseudorabies virus recombinants. J. Virol. 1999, 73:9521-9531.

21. Nakamura, K.; Morrison, S. F. Preoptic mechanism for cold-defensive responses to skin cooling. J. Physiol 2008, 586:2611-2620.

22. Leitner, C.; Bartness, T. J. Acute brown adipose tissue temperature response to cold in monosodium glutamate-treated Siberian hamsters. Brain Res 2009, 1292:38-51.

23. Nautiyal, K. M.; Dailey, M. J.; Brito, N. A.; Brito, M. N.; Harris, R. B. S.; Bartness, T. J.; Grill, H. J. Energetic responses to cold temperatures in rats lacking forebrain-caudal brainstem connections. Am. J. Physiol 2008, 295:R789-R798.

24. Morrison, S. F.; Madden, C. J.; Tupone, D. Central control of brown adipose tissue thermogenesis. Front Endocrinol. (Lausanne) 2012, 3.

25. Chen, X. M.; Nishi, M.; Taniguchi, A.; Nagashima, K.; Shibata, M.; Kanosue, K. The caudal periaqueductal gray participates in the activation of brown adipose tissue in rats. Neurosci. Lett. 2002, 331:17-20.

26. Kobayashi, A.; Osaka, T. Involvement of the parabrachial nucleus in thermogenesis induced by environmental cooling in the rat. Pflugers Arch. 2003, 446:760-765.

27. Cao, W. H.; Madden, C. J.; Morrison, S. F. Inhibition of brown adipose tissue thermogenesis by neurons in the ventrolateral medulla and in the nucleus tractus solitarius. Am. J Physiol Regul. Integr. Comp Physiol 2010, 299:R277-R290.

28. Taniguchi, A.; Chen, X. M.; Nagashima, K.; Tanaka, M.; Kanosue, K. Involvement of the raphe pallidus in the suppressive effect of preoptic warming on non-shivering thermogenesis in rats. Brain Res. 2003, 966:103-109.

29. Mantyh, P. W. The ascending input to the midbrain periaqueductal gray of the primate. J. Comp Neurol. 1982, 211:50-64.

30. Pechura, C. M.; Liu, R. P. Spinal neurons which project to the periaqueductal gray and the medullary reticular formation via axon collaterals: a double-label fluorescence study in the rat. Brain Res. 1986, 374:357-361.

31. Ter Horst, G. J.; de, B. P.; Luiten, P. G.; van Willigen, J. D. Ascending projections from the solitary tract nucleus to the hypothalamus. A Phaseolus vulgaris lectin tracing study in the rat. Neuroscience 1989, 31:785-797.

32. Moga, M. M.; Herbert, H.; Hurley, K. M.; Yasui, Y.; Gray, T. S.; Saper, C. B. Organization of cortical, basal forebrain, and hypothalamic afferents to the parabrachial nucleus in the rat. J. Comp Neurol. 1990, 295:624-661.

33. Petrovicky, P.; Kadlecova, O.; Masek, K. Mutual connections of the raphe system and hypothalamus in relation to fever. Brain Res. Bull. 1981, 7:131-149.

34. Petrovicky, P.; Kadlecova, O.; Masek, K. Reciprocal connection of the raphe system and the hypothalamus and their relationship to thermoregulation. Folia Morphol. (Praha) 1981, 29:180-182.

35. Grill, H. J.; Hayes, M. R. Hindbrain neurons as an essential hub in the neuroanatomically distributed control of energy balance. Cell Metab 2012, 16:296-309.

36. Song, C. K.; Schwartz, G. J.; Bartness, T. J. Anterograde transneuronal viral tract tracing reveals central sensory circuits from white adipose tissue. Am. J. Physiol Regul. Integr. Comp Physiol 2009, 296:R501-R511.

37. Brito, N. A.; Brito, M. N.; Bartness, T. J. Differential sympathetic drive to adipose tissues after food deprivation, cold exposure or glucoprivation. Am. J. Physiol Regul. Integr. Comp Physiol 2008, 294:R1445-R1452.

38. Souza, S. C.; Christoffolete, M. A.; Ribeiro, M. O.; Miyoshi, H.; Strissel, K. J.; Stancheva, Z. S.; Rogers, N. H.; D'Eon, T. M.; Perfield, J. W.; Imachi, H.; Obin, M. S.; Bianco, A. C.; Greenberg, A. S. Perilipin regulates the thermogenic actions of norepinephrine in brown adipose tissue. J Lipid Res. 2007, 48:1273-1279.

39. Puchalski, W.; Bocker, H.; Heldmaier, G.; Langefeld, M. Organ blood flow and brown adipose tissue oxygen consumption during noradrenaline-induced nonshivering thermogenesis in the Djungarian hamster. J. Exp. Zool. 1987, 242:263-271.

40. Baron, D. M.; Clerte, M.; Brouckaert, P.; Raher, M. J.; Flynn, A. W.; Zhang, H.; Carter, E. A.; Picard, M. H.; Bloch, K. D.; Buys, E. S.; Scherrer-Crosbie, M. In vivo noninvasive

characterization of brown adipose tissue blood flow by contrast ultrasound in mice. Circ. Cardiovasc. Imaging 2012, 5:652-659.

41. Foster, D. O.; Frydman, M. L. Nonshivering thermogenesis in the rat II. Measurements of blood flow with microspheres point to brown adipose tissue as the dominant site of the calorigenesis induced by noradrenaline. Can. J. Physiol. Pharmacol. 1978, 56:110-122.

42. Holzer, P. Efferent-like roles of afferent neurons in the gut: Blood flow regulation and tissue protection. Auton. Neurosci. 2006, 125:70-75.

43. Loesch, A. Perivascular nerves and vascular endothelium: recent advances. Histol. Histopathol. 2002, 17:591-597.

44. Borzan, J.; LaGraize, S. C.; Hawkins, D. L.; Peng, Y. B. Dorsal horn neuron response patterns to graded heat stimuli in the rat. Brain Res 2005, 1045:72-79.